OPEN ACCESS Freely available online

PLOS ONE

# Arsenic Removal from Aqueous Solutions Using $Fe_3O_4$-HBC Composite: Effect of Calcination on Adsorbents Performance

**Shams Ali Baig, TianTian Sheng, Chen Sun, XiaoQin Xue, LiSha Tan, XinHua Xu***

Department of Environmental Engineering, College of Environmental and Resource Sciences, Zhejiang University, Hangzhou, Zhejiang Province, China

## Abstract

The presence of elevated concentration of arsenic in water sources is considered to be health hazard globally. Calcination process is known to change the surface efficacy of the adsorbent. In current study, five adsorbent composites: uncalcined and calcined $Fe_3O_4$-HBC prepared at different temperatures (400°C and 1000°C) and environment (air and nitrogen) were investigated for the adsorptive removal of As(V) and As(III) from aqueous solutions determining the influence of solution's pH, contact time, temperature, arsenic concentration and phosphate anions. Characterizations from FTIR, XRD, HT-XRD, BET and SEM analyses revealed that the $Fe_3O_4$-HBC composite at higher calcination temperature under nitrogen formed a new product (fayalite, $Fe_2SiO_4$) via phase transformation. In aqueous medium, ligand exchange between arsenic and the effective sorbent site (=FeOOH) was established from the release of hydroxyl group. Langmuir model suggested data of the five adsorbent composites follow the order: $Fe_3O_4$-HBC-1000°C($N_2$)>$Fe_3O_4$-HBC (uncalcined)>$Fe_3O_4$-HBC-400°C($N_2$)>$Fe_3O_4$-HBC-400°C(air)>$Fe_3O_4$-HBC-1000°C(air) and the maximum As(V) and As(III) adsorption capacities were found to be about 3.35 mg $g^{-1}$ and 3.07 mg $g^{-1}$, respectively. The adsorption of As(V) and As(III) remained stable in a wider pH range (4–10) using $Fe_3O_4$-HBC-1000°C($N_2$). Additionally, adsorption data fitted well in pseudo-second-order ($R^2$>0.99) rather than pseudo-first-order kinetics model. The adsorption of As(V) and As(III) onto adsorbent composites increase with increase in temperatures indicating that it is an endothermic process. Phosphate concentration (0.0l mM or higher) strongly inhibited As(V) and As(III) removal through the mechanism of competitive adsorption. This study suggests that the selective calcination process could be useful to improve the adsorbent efficiency for enhanced arsenic removal from contaminated water.

**Citation:** Baig SA, Sheng T, Sun C, Xue X, Tan L, et al. (2014) Arsenic Removal from Aqueous Solutions Using $Fe_3O_4$-HBC Composite: Effect of Calcination on Adsorbents Performance. PLoS ONE 9(6): e100704. doi:10.1371/journal.pone.0100704

**Editor:** Vipul Bansal, RMIT University, Australia

**Received** February 19, 2014; **Accepted** May 27, 2014; **Published** June 26, 2014



**Funding:** The authors acknowledge the financial support of the National Natural Science Foundation (No. 21277119) and the Science and Technology Project of Zhejiang Province, China (No. 2012C23061). The funders had no role in study design, data collection and analysis, decision to publish, or preparation of the manuscript.

**Competing Interests:** The authors have declared that no competing interests exist.

* Email: xuxinhua@zju.edu.cn

## Introduction

Arsenic is an ubiquitous element that has been recognized to exist in four oxidation states (−3, 0, +3 and +5). Owing to its multiple toxic effects, arsenic has received considerable attention globally [1]. Chronic exposures to arsenic may cause various toxic events in humans including cancers of liver, lung and bladder. Over 200 million people worldwide are reported to be exposed to high concentrations of arsenic via contaminated water creating a major global health concern [2,3]. However, the World Health Organization (WHO) has reduced the recommended dose of arsenic in drinking water to 10 μg $L^{-1}$ [3]. In the past, numerous arsenic remediation techniques have been documented [2,4–9] including oxidation, coagulation and filtration, prcipitation and others [7,10,11]. Most of these techniques are technically more complex and normally associated with mixing of different chemicals which results in the generation of huge amounts of hazardous sludge for disposal [10–12].

One of the remediation techniques used against arsenic contamination is the adsorption technique which is considered to be highly effective for arsenic removal from water environments. The main advantages of this technique include its simple operation, economic reliability and least waste generation properties [8,12]. Various adsorbents developed from different cost-effective sources have been successfully tested so far [2,5,8,13]. Few highly adsorptive capacity nanostructure sorbents have been investigated in past years [14]; however, iron and its compounds, including iron oxides and iron hydroxides have shown more effective in arsenic removal [15]. In addition, from few of the recently reported studies, iron-oxide based composite sorbents were found to be most efficient as compared to other oxides or hydroxides [6,16,17]. For example, Luo et al. [6] utilized $Fe_3O_4$-reduced graphite oxide-$MnO_2$ nanocomposite for arsenic removal. Similarly, Feng et al. [17] developed superparamagnetic high-surface-area $Fe_3O_4$ nanoparticles for the same purpose and their results also confirmed the efficiency enhancement of iron oxide based composite sorbents.

Honeycomb briquette cinders (HBC) are waste biomass materials produced from household-based cylindrical stoves in many countries including China. Recently, the scientific applicability and the attractive surface compositions of HBC for pollutant remediation have been extensively investigated [8,18]. Previously,

we had successfully employed iron amended HBC (Fe-HBC) as an adsorbent for arsenic removal in aqueous and column-based studies [5,8]. It was found that the process of adsorption was significantly influenced by the adsorbent specific surface area and effective component compositions. To improve the surface properties of the absorbent, the process of calcination has been reported as one of the effective methods which can help to increase adsorbent hardness and decrease its water adhesion preventing the breakage of absorbent [19]. Generally, high temperature calcination process has shown to enhance adsorbent surface capacity and deformation of surface textural and mineralogical properties [20]. In contrast, Mahmood et al. [21] reported a decrease in arsenic adsorption efficiency by mixed oxide due to increased calcination temperature which resulted in decreasing the surface area of the adsorbent. However, the influence of calcination environments (air or nitrogen) and temperatures (lower or higher) on adsorbent composites for As(V) and As(III) removal has been rarely discussed in literature. Thereby, the optimal calcination temperature and environment for adsorbent development still needs to be elucidated.

In our current work, we evaluated the adsorption performance of calcined and uncalcined $Fe_3O_4$-HBC composites prepared at different temperatures (400°C and 1000°C) and environments (air and nitrogen) for the removal of As(V) and As(III) from aqueous solutions. The surface texture of $Fe_3O_4$-HBC composite and mineralogical variations were studied using XRD, HT-XRD, FTIR, BET and SEM techniques. The present study is an attempt to investigate the adsorption capacity of $Fe_3O_4$-HBC composites (uncalcined and calcined) for As(V) and As(III) from aqueous solutions which may help to elucidate the influence of solution pH, As(V) and As(III) concentration, calcination environment, contact time, temperature and the effects of phosphate anions.

## Materials and Methods

### Reagents

Chemicals including $FeSO_4.7H_2O$, $FeCl_3.6H_2O$, thiourea, L-ascorbic acid, potassium borohydride, hydrochloric acid solution, potassium di-hydrogen phosphate, $Na_3AsO_4.12H_2O$ and $Na_3AsO_3$ were all analytical grades and used without any purification. These chemicals were obtained from two dealers; i) Sinopharm Group Chemical Reagent Co., Ltd., China, and ii) Aladdin Chemistry Co., Ltd., Shanghai, China. As(V) and As(III) stock solutions (1000 mg $L^{-1}$) were prepared by dissolving the weighted amount of $Na_3AsO_4.12H_2O$ and $Na_3AsO_3$, respectively, in the measured volume of de-ionized (DI) water.

### Preparation of raw and calcined $Fe_3O_4$-HBC composite

Wastes HBC biomass materials were obtained from a local restaurant at Hangzhou city in China and widely available in both cities and rural settlements. Initially, the brownish color HBC were crushed with a hammer and then sieved to obtain <0.5 mm granules. The sieved granules were washed several times with acid and DI water, and then dried in oven at 50°C for 24 h. The dried HBC<0.5 mm granules were purposively used to fabricate with $Fe_3O_4$.

The $Fe_3O_4$-HBC composite was synthesized by a modified *in situ* chemical co-precipitation method, which has been employed for $Fe_3O_4$ generation [16]. Briefly, 5 g of HBC was added to a 100 mL mixed solution of $FeSO_4.7H_2O$ (2.78 g) and $FeCl_3.6H_2O$ (5.40 g) under nitrogen flow. Additionally, the proportionate amount of ammonia was poured by drop wise addition and the reaction was held for 2 h at 60°C temperature. The fabricated $Fe_3O_4$-HBC composite was washed with DI water for several times to remove unnecessary ions. The final adsorbent was then dried in vacuum at 60°C for 24 h. Afterwards, the dried $Fe_3O_4$-HBC composite was calcined in high temperature furnace under different conditions for 2 h to obtain the other four adsorbent composites; 1) uncalcined $Fe_3O_4$-HBC composite, 2) calcined at 400°C under air ($Fe_3O_4$-HBC-400°C(air)), 3) calcined at 400°C under nitrogen ($Fe_3O_4$-HBC-400°C($N_2$)), 4) calcined at 1000°C under air ($Fe_3O_4$-HBC-1000°C(air)) and 5) calcined at 1000°C under nitrogen ($Fe_3O_4$-HBC-1000°C ($N_2$)).

### Batch adsorption experiments

In this study, the effects of initial pH, equilibrium time, temperature, As(V) or As(III) concentration, kinetic and adsorption isotherms were investigated. Batch adsorption experiments were performed in a series of 100 mL glass conical flasks containing As(V) or As(III) aqueous solutions with 0.02 g calcined and uncalcined $Fe_3O_4$-HBC composite at 25±0.8°C. For adsorption experiments, 0.02 g calcined and uncalcined $Fe_3O_4$-HBC composite adsorbents were suspended in As(V) or As(III) aqueous medium with known concentrations and shaken with a speed of 150 rpm for 14 h. Afterwards, the suspensions were filtered using 0.45 μm filter membranes and the filtrate was subjected to analysis for the remaining total arsenic concentration. The adsorption capacity ($q_e$) and removal efficiency (RE (%)) were calculated using equations (1) and (2):

$$q_e = \frac{(C_0 - C_e)V}{m} \quad (1)$$

$$RE = \frac{(C_i - C_f)}{C_i} X100 \quad (2)$$

where $C_0$ and $C_i$ represent the initial As(V) or As(III) concentration, and $C_e$ and $C_f$ are the equilibrium or final concentration of the respective arsenic species in aqueous solution. V and m represent the volume of the aqueous solution and adsorbent mass, respectively.

Experiments for the kinetics of five $Fe_3O_4$-HBC adsorbent composites were performed by adding 0.02 g of adsorbent into 100 mL arsenic solution with the initial concentration of 100 μg $L^{-1}$ at pH 7.0. Samples were taken out at certain intervals using syringes and filtered. The effects of various pH values (pH 2–12) on As(V) and As(III) adsorption were performed by adjusting the aqueous solution pH using HCl and NaOH in 14 h contact time. Experiments for the equilibrium adsorption isotherms were performed with different initial arsenic concentrations containing 0.02 g of adsorbent at pH 7.0. The influence of temperature on As(V) and As(III) adsorption was investigated by varying the aqueous solution temperatures (25°C, 35°C and 45°C). Moreover, the effects of different $PO_4^{3-}$ concentrations on arsenic removal were investigated by adding different concentrations (0–1 mM) of phosphate into arsenic containing solutions. Each sample was tested in triplicates and the mean values were expressed with standard error.

### Adsorbents characterization

Fourier transform infrared spectroscopy (FTIR) of calcined and uncalcined adsorbent composites was recorded at 4000 and 400 $cm^{-1}$ wavenumber (IR Prestige-21, Japan). Scanning electron micrograph (SEM) (Hitachi S-3000N, Japan) was used to analyze the morphological structures of $Fe_3O_4$-HBC composite before and after calcination at different temperatures and environments. X-

ray diffraction (XRD) analysis (X'pert PRO analytical B.V., Netherlands) of the adsorbent composites was performed. In order to investigate the phase transformation of the adsorbent composite ($Fe_3O_4$-HBC-1000°C($N_2$)) *in situ* high temperature-X-ray diffraction (HT-XRD) (PANalytical, X'Pert PRO, Philips, Almelo, Netherlands) was performed at the heating rate of 10°C $min^{-1}$ under nitrogen environment and HT-XRD data were taken after heating at 1000°C. Brunauer–Emmett–Teller (BET) surface area of the samples was measured using BET surface analyzer (ASAP 2050, Micrometrics, Beijing, China).

### Analytical methods

Atomic fluorescence spectroscopy (model AFS-230E, Beijing Kechuang Haiguang Instrument Company, China) was used for the determination of total arsenic concentration [5,8]. The total arsenic detection limits and repeatability in AFS were 1 μg $L^{-1}$ and 10%, respectively. A digital pH meter (Mettler Toledo SG2, Shangai, China) was used to measure solution pH. High temperature furnace (model: GSL1500X Hefei, China) with the heating rate of 10°C $min^{-1}$ was used to calcine $Fe_3O_4$-HBC composite at 400°C and 1000°C under nitrogen flow and in static air (200 cc $min^{-1}$).

## Results and Discussion

### Characterization of adsorbent composites

The XRD patterns of the five $Fe_3O_4$-HBC adsorbent composites are presented in Fig. 1. The XRD peaks obtained revealed that quartz and magnetite were the major phases in uncalcined $Fe_3O_4$-HBC composite (Fig. 1a) and consistent with the corresponding values [8,18]. It was observed that with the increase in calcination temperature, there was an increase in the intensities of quartz and magnetite as shown in Fig 1b–d. Major peaks of quartz and magnetite were observed to appear at 2$\theta$ (20.8°, 26.6°, 39.4°, 50.1° and 59.6°) and 2$\theta$ (24.1°, 33.1°, 54.1° and 62.4°), respectively. During high temperature calcination under air some of the magnetite was oxidized into hematite and the new peaks appeared were marked "+" in the XRD pattern (Fig. 1d). Higher calcination temperature exhibited a significant effect on phase transformation, especially at 1000°C under nitrogen. Thus, most of the quartz and magnetite phases disappeared and formed a new product, fayalite ($Fe_2SiO_4$) as a major phase with the peaks appearing at 2$\theta$ (25.0°, 31.5°, 34.9°, 35.3°, and 51.1°) (Fig. 1e). High temperature calcination of quartz and magnetite under nitrogen environment has been recognized to favor the formation of fayalite [22,23]. HT-XRD analysis of the adsorbent composite ($Fe_3O_4$-HBC-1000°C($N_2$)) also confirmed the formation of fayalite (Fig. S1) and there was an increase in the relative intensity of fayalite recorded at 1000°C under nitrogen environment as compared to XRD patterns (Fig. 1e). In such anhydrous environment, oxygen fugacity was found to be very low to maintain the stability of ferrous iron to react with silicate. In contrast, high temperature calcination under air can produce magnetite and silicate from fayalite [24]. From this study it revealed that the high temperature calcination under controlled environment would only guarantee phase transformation, as shown in Fig. 1e. But the low temperature (400°C) calcination under nitrogen environment cannot favor the formation of fayalite (Fig. 1c).

The presence of different functional groups on the adsorbent was analyzed by FTIR analysis (Fig. 2). The appearance of band at 475 $cm^{-1}$ was attributed to Fe-O vibration, which was observed to become stronger with the increase in the calcination temperature. However, H-O-H bonding in water was assumed to be responsible

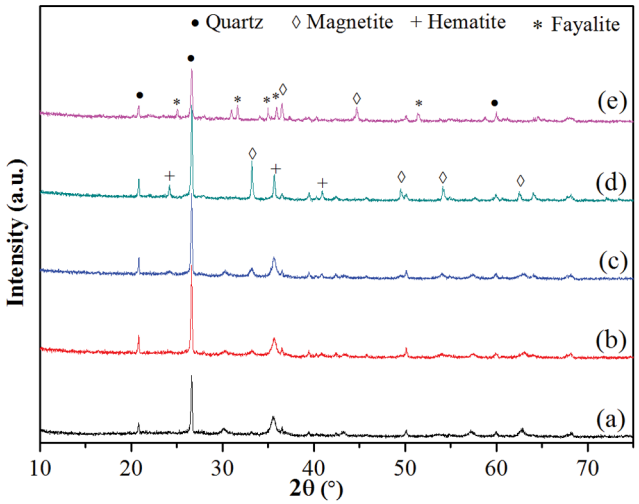


**Figure 1. XRD pattern of five adsorbent composites: (a) uncalcined $Fe_3O_4$-HBC composite, (b) 400°C under air, (c) 400°C under nitrogen, (d) 1000°C under air, and (e) 1000°C under nitrogen. Different XRD peaks are also marked.**
doi:10.1371/journal.pone.0100704.g001

for the appearance of band at 1550 $cm^{-1}$. Moreover, a strong band was found to appear at 1091 $cm^{-1}$ in the FTIR spectra (Fig. 2a–d) representing Si-O-Si stretching mode. The band observed around 1036 $cm^{-1}$ and 1098 $cm^{-1}$ in $Fe_3O_4$-HBC-1000°C($N_2$) confirmed the fayalite formation [23]. Sharp peak and broader absorption bands observed at 2976 $cm^{-1}$ and 3435 $cm^{-1}$ in $Fe_3O_4$-HBC-1000°C($N_2$) could be assigned to C-H stretching vibration and $OH^-$ vibrational modes, respectively. Moreover, C-H stretching vibration band in the same adsorbent reflected the presence of absorbing carbon [25].

Increase in calcination temperature resulted in coarsening of particles due to sintering processes [20]. According to SEM images shown in Fig. 3a–e, it can be seen that the calcined $Fe_3O_4$-HBC composite at 400°C and 1000°C, showed polyhedral and heterogeneous particles size distributions. But there were some morphological and mineralogical differences observed in adsor-

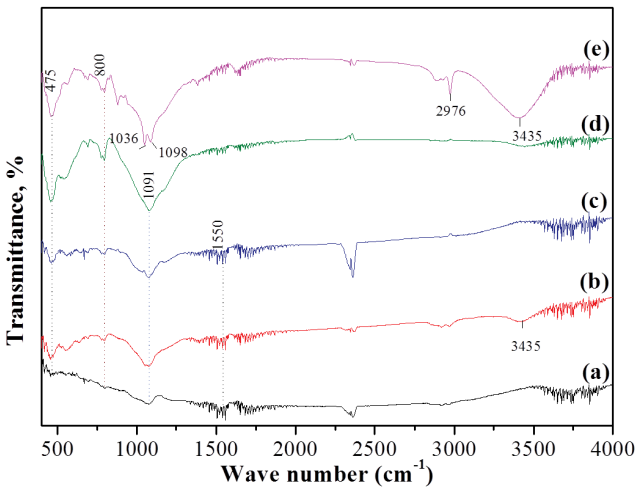


**Figure 2. FTIR spectra of (a) uncalcined $Fe_3O_4$-HBC composite, (b) 400°C under air, (c) 400°C under nitrogen, (d) 1000°C under air, (e) 1000°C under nitrogen.**
doi:10.1371/journal.pone.0100704.g002

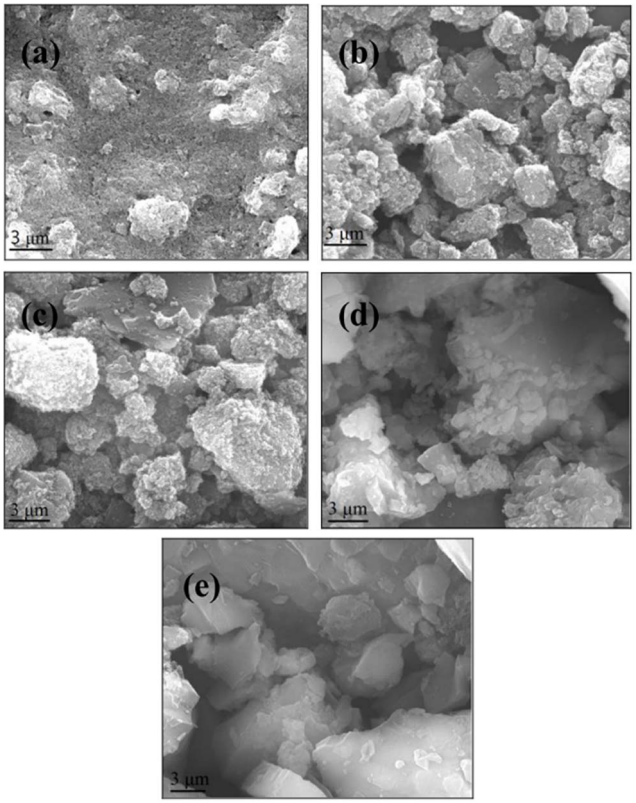


**Figure 3. SEM images of (a) uncalcined $Fe_3O_4$-HBC composite, (b) 400°C under air, (c) 400°C under nitrogen, (d) 1000°C under air, (e) 1000°C under nitrogen.**
doi:10.1371/journal.pone.0100704.g003

bents calcined under air and nitrogen flow. It has been suggested that elevated calcination temperature can remove water and organics from the adsorbent and tends to sinter and crystallize, which cause to decrease the surface area [26]. In our study, the surface area of all the calcined adsorbents were drastically decreased from 33.05 ($m^2$ $g^{-1}$) of $Fe_3O_4$-HBC (uncalcined) to 0.04, 0.03, 0.95 and 6.03 ($m^2$ $g^{-1}$) of $Fe_3O_4$-HBC-400°C($N_2$), $Fe_3O_4$-HBC-400°C(air), $Fe_3O_4$-HBC-1000°C(air), $Fe_3O_4$-HBC-1000°C($N_2$), respectively, as shown in Table 1. Additionally, the mean pore diameter of the adsorbents also greatly varied from each other (Table 1).

Generally, sintering is known to start between 100°C and 300°C, but the most extensive crystallization processes could take place in between 500–700°C, where the porosity and surface area may markedly decrease [20]. Similarly, Kurtoglu et al. [25] found that stronger and clear bands were only appeared at a maximum calcination temperature (i.e. 1000°C). In this study, calcination at 1000°C under nitrogen resulted in the formation of a new iron silicate product (fayalite, $Fe_2SiO_4$) with an average pore diameter of 15.01 nm (Fig. 3e and Table 1). Moreover, the calcined products formed at 400°C under air and nitrogen nearly showed the same mean pore diameter and BET surface area (Table 1). But the adsorbent calcined at 1000°C showed significant annealing or textural modification from 400°C to 1000°C after 2 h of calcination. Nitrogen-calcined composite showed better phase transformation at higher temperature, as shown in XRD and HT-XRD patterns (Fig. 1e and Fig. S1). In contrast, insignificant annealing was also reported even at 800°C in run products (fayalite, magnetite and quartz) [26].

## Calcination environments and $Fe_3O_4$-HBC composite products

Magnetite and quartz were the major phases observed in the adsorbent composite, as revealed in XRD patterns (Fig. 1a). High temperature calcination (1000°C) under nitrogen generated a new iron silicate phase (fayalite, $Fe_2SiO_4$) (Fig. 1e and Fig. S1). Fayalite formation can be written, as Eq. (3) [22,23].

$$2Fe_3O_4 + 3SiO_2 \rightarrow 3Fe_2SiO_4 + O_2 \quad (3)$$

Fayalite is known to form in an environment where the oxygen fugacity is low enough to maintain the stability of ferrous iron [22]. Fayalite is the reaction product of magnetite and quartz under the reducing environment with low water content. In this study, the oven-dried $Fe_3O_4$-HBC composite was calcined and amount of water content was negligible. $Fe_3O_4$-HBC composite calcined at higher temperature under nitrogen contains significant amount of carbon from the carbonization of organic precursor, which can be reflected by C-H stretching vibration mode observed at 2976 $cm^{-1}$ in FTIR spectra (Fig. 2e). No C-H stretching vibration mode was recorded in the adsorbent calcined at high temperature under air indicating complete combustion of organic materials (Fig. 2d).

High temperature calcination under air signified the role of oxic-environment, which further enhanced magnetite and quartz contents in the adsorbent (Fig. 1d). Similarly, Michel et al. [24] reported that at high calcination temperature under air, the fayalite is known to be oxidized and form quartz and magnetite, according to the following reaction (Eq. (4)).

$$3Fe_2SiO_4 + O_2 \rightarrow 2Fe_3O_4 + 3SiO_2 \quad (4)$$

Correspondingly, Shahar et al. [26] reported that in oxygen fugacity buffer, a stable assemblage comprising of quartz-fayalite-

**Table 1.** Textural characteristics of uncalcined and calcined $Fe_3O_4$-HBC composites.

| Adsorbent | Surface area ($m^2$ $g^{-1}$) | Total pore volume $V_p$ ($cm^3$ $g^{-1}$) | Mean pore diameter (nm) |
|---|---|---|---|
| $Fe_3O_4$-HBC uncalcined | 33.05 | 0.0966 | 13.35 |
| 400°C under air | 0.04 | 0.0027 | 187.54 |
| 400°C under nitrogen | 0.03 | 0.0018 | 229.79 |
| 1000°C under air | 0.95 | 0.0851 | 31.73 |
| 1000°C under nitrogen | 6.03 | 0.0080 | 15.01 |

doi:10.1371/journal.pone.0100704.t001

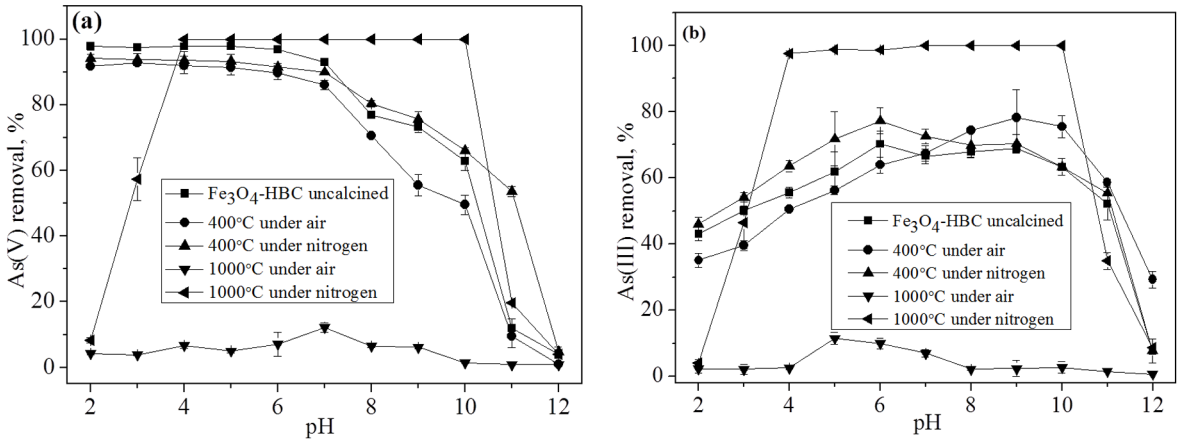


**Figure 4. Effects of initial solution pH on the removal of As(V) (a) and As(III) (b) (Experiment conditions: adsorbent dose = 0.02 g 100 mL$^{-1}$, temperature = 25±0.8°C, agitation speed = 150 rpm, initial concentration = 100 μg L$^{-1}$, contact time = 14 h).**
doi:10.1371/journal.pone.0100704.g004

magnetite (QFM) could be formed. But the fayalite stability analysis under different calcination environments was not within the scope of this study. However, further studies are required to measure the oxygen fugacity at elevated calcination temperature under air and its reaction with arsenic in contaminated water.

## Effect of solution pH

The effects of solution pH on As(V) and As(III) adsorption by calcined and uncalcined adsorbents were investigated at different pH values (2–12) (Fig. 4a and b). Arsenic adsorption is known to be pH-dependent, moreover, the surface groups of the adsorbent are also considered vulnerable to be protonated and deprotonated [9,16]. The removal efficiency of As(V) using uncalcined and calcined adsorbent composites at 400°C in both air and nitrogen, respectively, was decreased with the increase in the initial pH (Fig. 4a). Higher adsorption of arsenic at lower pH may be due to the electrostatic attraction of the positively charge adsorbent sites and the negatively charged $H_2AsO_4^-$ species. Generally, As(V) is known to exist in negative ionic form under most of the pH conditions [16]. Correspondingly, we can assume that at low pH the adsorbent composites should behave as weak acid and form positive surface site for anionic arsenic adsorption by forming inner-sphere surface complexes. However, As(V) removal efficiency was observed to drastically decrease above pH 7, which is in agreement with previous studies [6]. However, $Fe_3O_4$-HBC-1000°C($N_2$) showed the highest As(V) adsorption at wider pH range (4–10). In aqueous medium, $Fe_2SiO_4$ showed to form a highly reactive iron species (= FeOOH) [9,23] and that bound to As(V) and As(III) by ligand exchanges. The occurrence of ligand exchange between As(V) and As(III) with adsorbent effective site (= FeOOH) suggested the completion of sorption process by forming inner-sphere surface complexes at the solid-water interface, as written in Eqs. (5), (6) and (7).

$$Fe_2SiO_4 + \frac{1}{2}O_2 + 3H_2O \rightarrow 2[FeOOH] + 4H^+ + SiO_4^{4-} \quad (5)$$

$$FeOOH + As(V) + H^+ \rightarrow FeO - As(V) + H_2O \quad (6)$$

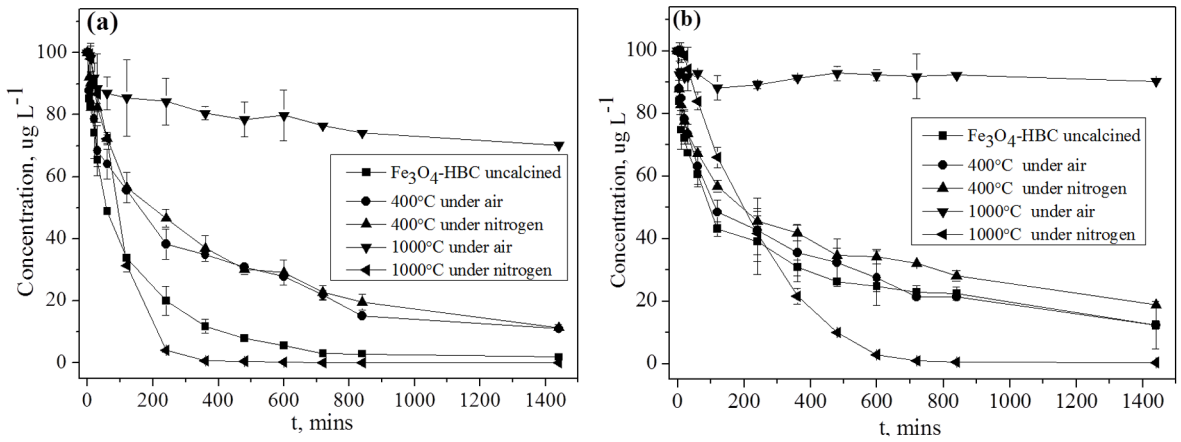


**Figure 5. The effect of contact time on the removal of As(V) (a) and As(III) (b) by the uncalcined and calcined $Fe_3O_4$-HBC composite (Experiment conditions: adsorbent dose = 0.02 g 100 mL$^{-1}$, temperature = 25±0.8°C, agitation speed = 150 rpm, initial concentration = 100 μg L$^{-1}$, contact time = 14 h).**
doi:10.1371/journal.pone.0100704.g005

**Table 2.** Comparisons of pseudo-first and pseudo-second-order models calculated reaction constants for uncalcined and calcined $Fe_3O_4$-HBC composites with the experimental data.

| Adsorbent | Arsenic species | Pseudo-first order kinetic model | | | Pseudo-second order kinetic model | | | Experimental data $q_e$(μg g$^{-1}$) |
|---|---|---|---|---|---|---|---|---|
| | | $k_1$(min$^{-1}$) | $q_e$(μg g$^{-1}$) | $R^2$ | $k_2$ (g mg$^{-1}$ min$^{-1}$) | $q_e$(μg g$^{-1}$) | $R^2$ | |
| $Fe_3O_4$-HBC uncalcined | As(V) | 0.0023 | 13.0 | 0.9808 | 0.0428 | 564.1 | 0.9984 | 547.4 |
| 400°C under air | As(V) | 0.0008 | 12.0 | 0.9233 | 0.0117 | 387.2 | 0.9930 | 404.2 |
| 400°C under nitrogen | As(V) | 0.0011 | 13.0 | 0.9796 | 0.1978 | 476.0 | 0.9900 | 500.0 |
| 1000°C under air | As(V) | 0.0008 | 08.0 | 0.8985 | 0.0794 | 132.4 | 0.9809 | 150.2 |
| 1000°C under nitrogen | As(V) | 0.0049 | 15.0 | 0.9889 | 0.0182 | 628.1 | 0.9917 | 552.1 |
| $Fe_3O_4$-HBC uncalcined | As(III) | 0.0010 | 11.0 | 0.9816 | 0.0461 | 371.4 | 0.9964 | 401.0 |
| 400°C under air | As(III) | 0.0011 | 12.0 | 0.9271 | 0.0255 | 390.4 | 0.9924 | 401.2 |
| 400°C under nitrogen | As(III) | 0.0009 | 11.0 | 0.9657 | 0.0329 | 340.0 | 0.9939 | 366.2 |
| 1000°C under air | As(III) | 0.0004 | 02.0 | 0.1832 | 15.755 | 6.1 | 0.9695 | 9.76 |
| 1000°C under nitrogen | As(III) | 0.0032 | 18.0 | 0.9817 | 0.0034 | 806.4 | 0.9960 | 560.2 |

doi:10.1371/journal.pone.0100704.t002

$$FeOOH + As(III) + H^+ \rightarrow FeO - As(III) + H_2O \quad (7)$$

$Fe_3O_4$-HBC-1000°C(air) showed to have the lowest efficiency (<10%) at the studied pH range (2–12) (Fig. 4a). Variations of the effective surface component at high calcination temperature enabled the adsorbent as an efficient agent for treating arsenic contaminated water. The removal efficiency of As(III) reached to nearly 70% at pH 6 for $Fe_3O_4$-HBC-400°C($N_2$) and was observed to decrease at both low and high pH values (Fig. 4b), as reported earlier [27]. Generally, As(III) exists as neutral species at pH<9.2 that can be deprotonated to form more negatively charged anions ($H_2AsO_3^-$) [7]. The reduction in arsenic removal with the increase in the solution pH could be attributed to the electrostatic repulsion of the negatively charged adsorbent surface from the anionic $H_2AsO_4^-$, $HAsO_4^{2-}$ and $H_2AsO_3^-$ species [7,21]. Consequently, the combined effects of enhanced electrostatic repulsion and the hydroxyl ion competition can be accounted responsible for the declined arsenic removal in alkaline aqueous conditions. However, the efficient removal of As(V) and As(III) by $Fe_3O_4$-HBC-1000°C($N_2$) might be the result of the surface component ($SiO_4^{4-}$), which further resulted in enhanced adsorption within a wider pH range (pH 4–10). The final solution pH in case of adsorbent ($Fe_3O_4$-HBC-1000°C($N_2$)) showed considerable increase at equilibrium for both As(V) and As(III) as compared to other adsorbent composites (Fig. S2).

## Effect of contact time and adsorption kinetics

Generally, adsorption onto the adsorbent from aqueous solution involves three steps, namely; 1) transport into the exterior surface (film diffusion), 2) transport into the pore and surface diffusion (intraparticle diffusion), and 3) adsorption onto the adsorbent surface from the bulk phase. Hence, the overall adsorption rate is determined by the slowest adsorption step involved [28]. Fig. 5a and b presents As(V) and As(III) removal using five adsorbent composites along with contact times. All the adsorbents except $Fe_3O_4$-HBC-1000°C(air) were found significantly effective for the removal of both As(V) and As(III), especially $Fe_3O_4$-HBC-1000°C($N_2$). But $Fe_3O_4$-HBC (uncalcined), $Fe_3O_4$-HBC-400°C($N_2$) and $Fe_3O_4$-HBC-400°C(air) demonstrated over 80% removal efficiencies for both As(V) and As(III). Rapid reduction was recorded in the first 4 h for both As(V) and As(III), which subsequently slowed down and reached to equilibrium within 14 h contact time. This could be attributed to the phenomenon that higher concentration gradient and more adsorptive sites favor fast adsorption initially. However, when the adsorption experiments were extended up to 24 h, no significant adsorption was observed (Fig. 5a and b).

Adsorption kinetics depends on the interaction of adsorbate-adsorbent in aqueous adsorption system and plays an important role in water purification measures. Reaction rate and adsorption mechanism are the two key elements in adsorption process. The uptake of solute rate determines the retention time required to complete the adsorption process, which can be enumerated from kinetic studies. Numerous models can be employed to express the solute adsorption onto an adsorbent [29,30]. In order to investigate the adsorption mechanism, characteristic constants, and the solid phase adsorption pseudo-first order (PFO) [29] and pseudo-second order (PSO) kinetics models [30] can be used. Thus, in this study PFO and PSO models were introduced to fit the adsorption kinetics of As(V) and As(III) onto uncalcined and calcined $Fe_3O_4$-HBC composites (Fig. S3). The PFO and PSO adsorption kinetics equations are presented in Eqs. (8) and (9):

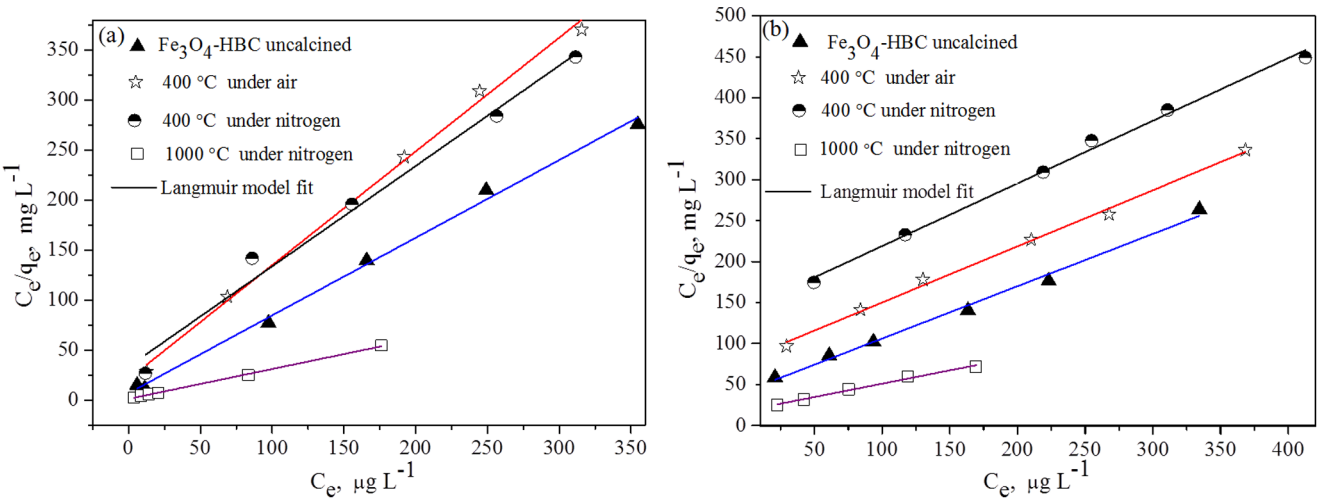


**Figure 6. Adsorption isotherm parameters for As(V) (a) and As(III) (b) adsorption onto calcined and uncalcined $Fe_3O_4$-HBC composite at pH 7.0 and temperature (25±0.8°C).**
doi:10.1371/journal.pone.0100704.g006

$$\ln(q_e - q_t) = \ln q_e - k_1 . t \quad (8)$$

$$\frac{t}{q_t} = \frac{1}{(k_2 . q_e^2)} - \frac{1}{q_e} t \quad (9)$$

where $q_e$ and $q_t$ (mg $g^{-1}$) are the amount of solute adsorbed per unit mass of adsorbent at equilibrium time t (min), $k_1$ ($min^{-1}$) is the PFO adsorption rate constant, $k_2$ (g $mg^{-1}$ $min^{-1}$) is the PSO adsorption rate constant and $k_2.q_e^2$ (mg $g^{-1}$ $min^{-1}$) is the PSO adsorption rate at t = 0 (min). The parameters of kinetics model obtained from PFO and PSO calculations (Fig. S3) and experimental data are summarized in Table 2. According to Table 2, the adsorption of both As(V) and As(III) fitted well in PSO kinetics model ($R^2$>0.99) rather than PFO kinetics model ($R^2$>0.91) for all the adsorbents. Furthermore, the adsorption capacity ($q_t$) at any time t (min) of As(V) was found to be greater than that of As(III). The adsorption equilibrium amount $q_e$ (628 μg $g^{-1}$) predicted in the PSO kinetics model was observed to be similar to the experimental value (552 μg $g^{-1}$) (Table 2). Kinetic data revealed that the mechanisms for both As(V) and As(III) removal were complex and most likely all of the three aforementioned steps might be involved in the adsorption of arsenic onto the adsorbent from aqueous solutions. The fitted data in PSO kinetics model are assumed to follow chemisorption phenomenon [28]. However, with rate limited chemisorptions; the precipitation and inner-sphere complexation are known to be involved between the adsorbate and adsorbent.

## Effect of temperature

To study the effect of temperature on the adsorption capacity of the adsorbent composites is very important for designing a sustainable adsorption system. Our results demonstrated that with the increase in temperature from 25°C to 45°C, the adsorption capacities of the adsorbent composites were slightly increased (Table S1). This showed that the adsorption process is an endothermic and controlled by the intraparticle and pore diffusion [3,9]. The mobility of adsorbent ions increases with the increase of the aqueous temperature, thus increasing the adsorptive capacity of the adsorbent composites. Similarly, the adsorption capacity of magnetite-graphene hybrids for arsenic was found to be increased from 10°C to 30°C [27].

**Table 3.** Langmuir model parameters for the adsorption of As(V) and As(III) on $Fe_3O_4$-HBC composite at ambient temperature (25±0.8°C).

| Adsorbent | Arsenic species | Langmuir model parameters | | |
|---|---|---|---|---|
| | | $q_m$ (mg $g^{-1}$) | $k_1$ (L $mg^{-1}$) | $R^2$ |
| $Fe_3O_4$-HBC uncalcined | As(V) | 1.288 | 109.35 | 0.9754 |
| 400°C under air | As(V) | 0.880 | 54.13 | 0.9656 |
| 400°C under nitrogen | As(V) | 0.998 | 30.06 | 0.9801 |
| 1000°C under nitrogen | As(V) | 3.355 | 254.56 | 0.9988 |
| $Fe_3O_4$-HBC uncalcined | As(III) | 1.566 | 14.96 | 0.9811 |
| 400°C under air | As(III) | 1.460 | 8.38 | 0.9753 |
| 400°C under nitrogen | As(III) | 1.308 | 5.36 | 0.9740 |
| 1000°C under nitrogen | As(III) | 3.071 | 17.57 | 0.9984 |

doi:10.1371/journal.pone.0100704.t003

**Table 4.** Comparison of the adsorption capacities of different adsorbents for As(V) and As(III).

| Adsorbent | pH | Temperature(°C) | Arsenic removal (mg $g^{-1}$) | | Reference |
|---|---|---|---|---|---|
| | | | As(V) | As(III) | |
| Fe-HBC | 7.5 | 23±2 | 0.9 | - | [8] |
| Magnetic wheat straw (MWS) | 7.0 | 30 | 8.02 | 3.8 | [16] |
| Ascorbic acid-coated-$Fe_3O_4$ nanoparticles | 7.0 | 25 | 16 | 46 | [17] |
| Biochar/γ-F $e_2O_3$ composite | 7.0 | 22±0.5 | 3.1 | - | [34] |
| Natural iron ores | 6.5 | 25 | 0.4 | - | [36] |
| $Fe_3O_4$-HBC composite | 7.0 | 25±08 | 3.35 | 3.07 | This study |

doi:10.1371/journal.pone.0100704.t004

## Adsorption isotherm studies

To help optimize the process for removal of arsenic, it is important to understand arsenic distribution between phases via analyzing the equilibrium data. In this study, equilibrium adsorption isotherm studies were performed for four adsorbent composites: $Fe_3O_4$-HBC (uncalcined), $Fe_3O_4$-HBC-400°C($N_2$), $Fe_3O_4$-HBC-400°C(air) and $Fe_3O_4$-HBC-1000°C($N_2$). Langmuir model is valid for a monolayer sorption mechanism with homogeneous sorption energies [31]. Monolayer adsorption onto the adsorbent surface has finite number of similar sites. Generally, it is assumed that further metal ions adsorption could not take place once the surface is saturated from that ions [32]. The Langmuir model [31] can be expressed as Eq. (10).

$$\frac{C_e}{q_e} = \frac{1}{k_1 q_m} + \frac{C_e}{q_m} \quad (10)$$

where $C_e$ and $q_e$ are arsenic equilibrium concentrations and adsorption capacity (mg $g^{-1}$), respectively, based on the dry weight of the adsorbents. $k_1$ is the Langmuir adsorption equilibrium constant (L $mg^{-1}$) and $q_m$ is the maximum adsorption capacity (mg $g^{-1}$). The plot between $C_e/q_e$ (along y-axis) and $C_e$ (along x-axis) at different initial As(V) and As(III) concentrations showed to generate straight lines (Fig. 6a and b), which revealed that the adsorption process of As ions onto the adsorbent composites followed the Langmuir adsorption Eq. (10). However, more straight lines ($R^2$>0.99) were observed for As(V) as compared to As(III) (Table 3). This variation in adsorption isotherm studies might be the differences in adsorption free energies of As(V) and As(III) [16,32,33]. Generally, As(V) species ($H_2AsO_4^-$) is predominantly available in the studied aqueous solution pH (~7.0) which has lower free adsorption energy as compared to As(III) species ($H_3AsO_3$). Thus, the adsorption capacity of As(V) was found higher than that of As(III) which is in agreement with previously reported studies [25,27,34], but disgreement with study reported by Luo et al. [6]. The maximum calculated adsorption for As(V) followed the order: $Fe_3O_4$-HBC-1000°C($N_2$)>$Fe_3O_4$-HBC (uncalcined)>$Fe_3O_4$-HBC-400°C($N_2$)>$Fe_3O_4$-HBC-400°C(air). The maximum adsorption capacities ($q_m$) of $Fe_3O_4$-HBC-1000°C($N_2$) for As(V) and As(III) were recorded to be 3.37 mg $g^{-1}$ and 3.07 mg $g^{-1}$, respectively (Table 3). Hence, among the other adsorbents presented in Table 4, $Fe_3O_4$-HBC-1000°C($N_2$) was found highly effective than that of iron-amended adsorbents, but less efficient than that of $Fe_3O_4$-nanocomposites.

In Langmuir model, the isotherm curve is considered to estimate the sorption process in term of "favorable" and "unfavorable" [8]. Thus, the constant $k_1$ is related to the equilibrium parameter; $R_L$, which can be defined as [35]:

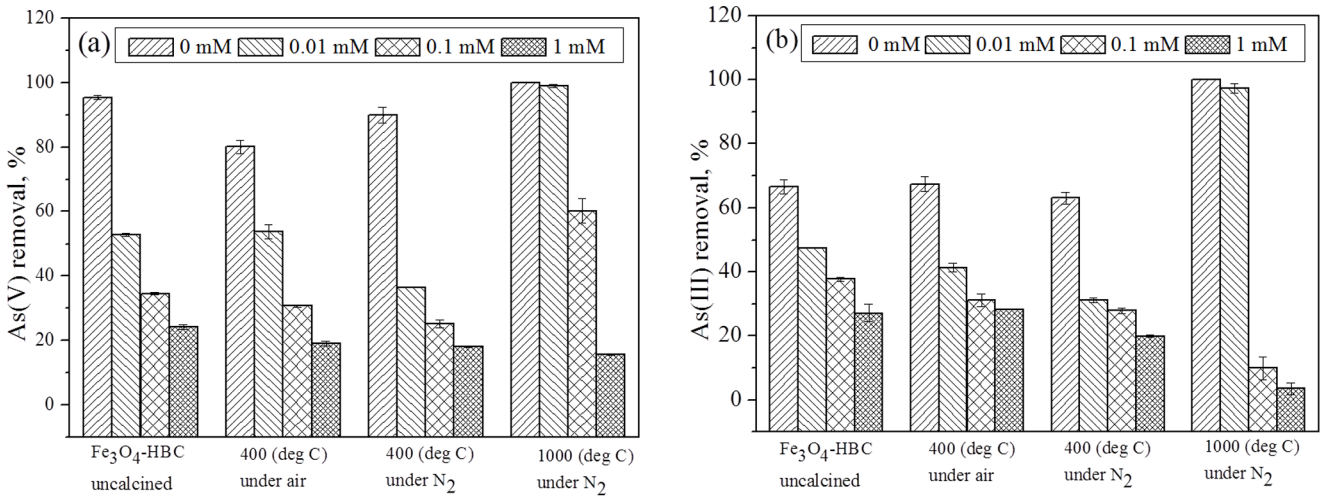


**Figure 7. Effect of phosphate concentrations (0–1 mM) on the adsorption of As(V) (a) and As(III) (b) using uncalcined and calcined $Fe_3O_4$-HBC composite.** Experiment conditions: adsorbent dose = 0.02 g 100 $mL^{-1}$, temperature = 25±0.8°C, agitation speed = 150 rpm, initial concentration = 100 μg $L^{-1}$, contact time = 14 h).
doi:10.1371/journal.pone.0100704.g007

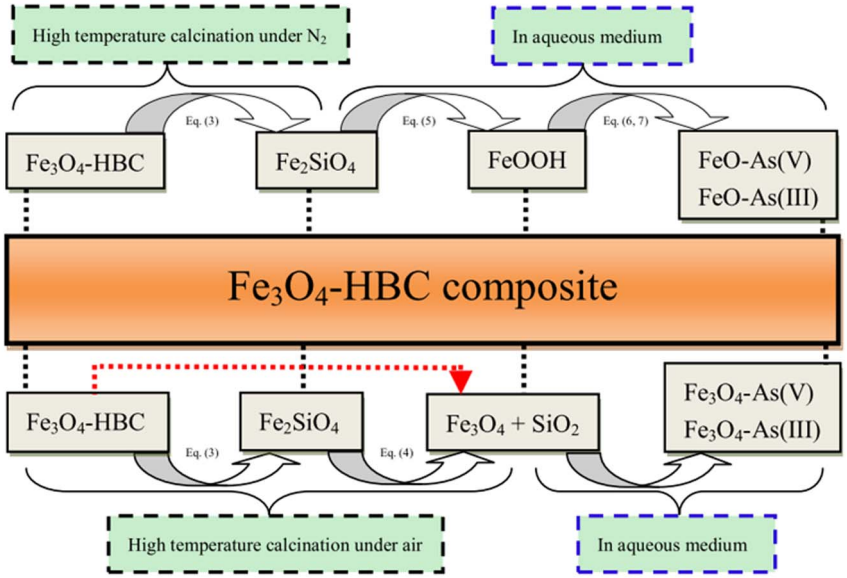


**Figure 8. The proposed removal mechanism for As(V) and As(III) in aqueous system.**
doi:10.1371/journal.pone.0100704.g008

$$R_L = \frac{1}{1 + k_1 C_0} \quad (11)$$

where $C_0$ (mg $L^{-1}$) is the initial concentration of As(V) and As(III). The values of $R_L$ for As(V) and As(III) within the studied $C_0$ range were observed to be 0.061–0.332 and 0.042–0.651, respectively. Therefore, the calculated values of "$R_L$" were found to be in between 0 and 1 indicating the adsorption of As(V) and As(III)onto uncalcined and calcined $Fe_3O_4$-HBC composite is a favorable process.

## Effects of phosphate anion on arsenic removal

The presence of phosphate in water is reported to significantly lower the ability of iron containing adsorbent to remove arsenic by adsorption [33]. Fig. 7a and b presents the interference study of different $PO_4^{3-}$ strengths (0–1 mM) on As(V) and As(III) adsorption from aqueous solutions using four composite adsorbents: $Fe_3O_4$-HBC (uncalcined), $Fe_3O_4$-HBC-400°C($N_2$), $Fe_3O_4$-HBC-400°C(air) and $Fe_3O_4$-HBC-1000°C($N_2$). Results showed that both As(V) and As(III) removal efficiencies decreased while increasing the phosphate concentration, which is in agreement with the studies reported by [33,36]. For example, Chowdhury and Yanful [33] trailed natural groundwater containing 5 mg $L^{-1}$ phosphate and 1.13 mg $L^{-1}$ arsenic, where only half of the arsenic was removed by mixed magnetite-maghemite nanoparticles. Phosphate is recognized for its interference in the binding of arsenic to various materials, similarly, in our study we found that phosphate concentration (0.01 mM or above) has a significant effect on the removal of both; As(V) and A(III). However, initially at lower concentration (~0.01 mM) of $PO_4^{3-}$, the binding of arsenic to $Fe_3O_4$-HBC1000°C($N_2$) remained to be unaffected. This clearly suggests that the low concentration of phosphate has weaker attraction due to the presence of surface component ($SiO_4^{4-}$), as written in Eq. (5). Moreover, 0.1 mM $PO_4^{3-}$ concentration exhibited significant As(V) removal efficiency (above 60%); however, it showed to remove only 10% of As(III) at the same $PO_4^{3-}$ concentration level (Fig. 7a and b).

Higher phosphate concentration has known to inhibit arsenic removal through the mechanisms of charged diffusion and competitive adsorption [9,37]. In addition, formation of more stable phosphate complexes ($Fe(H_2PO_4)_3$) with Fe(III) has been suggested another possible adsorption mechanism [38]. On the other hand, under same conditions, As(III) affinity towards uncalcined and calcined composite adsorbents was found to be weaker as compared to that of As(V) and phosphate. Consequently, the removal efficiency of As(III) was lowered and consistent with the findings reported in previous studies [9,39]. Moreover, our work showed the probable effect of solution pH, As(V) and As(III) concentrations, calcination environment, temperature, contact time and the effects of phosphate anions on As(V) and As(III) removal.

## Removal mechanism of arsenic

Fig. 8 presents the schematic possible mechanism of As(V) and As(III) adsorption from aqueous system. So far, various probable reaction pathways have been proposed for the adsorption mechanism of arsenic using different adsorbents; however, the mechanism of arsenic removal from aqueous solution is still partially understood [40]. In this study, a new iron silicate phase (fayalite, $Fe_2SiO_4$) was formed due to high temperature calcination under nitrogen environment, as discussed previously. The elevated calcination temperature is known to decrease the surface area and increase the particle size, which can ultimately decrease the removal performance [20,21]. The substantial changes in the surface area and mean pore diameter were noticed when the $Fe_3O_4$-HBC composite was calcined (Table 1). But in this study, when the newly formed fayalite (BET: 6.03 ($m^2$ $g^{-1}$)) was added into arsenic containing solutions, it resulted in the formation of a highly reactive iron species (=FeOOH). Therefore, the adsorbent mineralogical compositions played more important role for the removal of arsenic from aqueous solutions. In contrast, $Fe_3O_4$-HBC composite calcined at lower temperature (400°C) and oxygenated environment did not produce any reactive sites. Additionally, the surface area was also reduced to 0.95 $m^2$ $g^{-1}$ that further limited its removal performance. In aqueous medium, FeOOH (or hydrous ferric oxide, HFO) as a predominant

immobilized species on iron surface reacted with As(III) and As(V) through ligand exchange by forming Fe-As complexes, which was also shown in a recent study [23].

On the other hand, due to higher chemical potential of oxygen at elevated calcination temperature (1000°C) under air, the fayalite formed quartz and magnetite/hematite [24] (Fig. 1d) with apparent XRD peaks (Fig. 1d). Moreover, the absence of C-H stretching bonding in the FTIR spectra (Fig. 1d) revealed complete decomposition of organic materials. Consequently, it was found that the resulted bare $Fe_3O_4$ had lower As(V) and As(III) removal efficiencies, which is in agreement with the results reported earlier [7,16]. For example, Tian et al. [16] confirmed that the As(V) removal efficiency using bare $Fe_3O_4$ was only 6.98 mg $g^{-1}$ as compared to the wheat straw loaded with $Fe_3O_4$ (30.34 mg $g^{-1}$). Thus, they concluded that higher $Fe_3O_4$ content resulted to a higher arsenic adsorption capacity.

## Conclusions

To summarize, in current work, the synthesized $Fe_3O_4$-HBC composite was calcined at 400°C and 1000°C under air and nitrogen. High temperature calcination promoted phase transformation and formed a new iron silicate phase (fayalite, $Fe_2SiO_4$), which in turn generated highly reactive site (=FeOOH) in aqueous system. Thus, $Fe_3O_4$-HBC-1000°C($N_2$) showed higher removal efficiency for both As(V) and As(III) at a wider pH range (4–10) as compared to other adsorbent composites. The adsorption of As(V) and As(III) is an endothermic process and maximum adsorption capacity of adsorbent composites increases from 25°C to 45°C. The presence of elevated concentration of phosphate was found to strongly inhibit As(V) and As(III) adsorption. Furthermore, the possible adsorption mechanism was demonstrated. This study suggests that the selective calcination process can be useful to improve the adsorbent efficiency for enhanced arsenic removal from contaminated aqueous environments.

## Supporting Information

**Figure S1 HT-XRD patterns of the adsorbent composite ($Fe_3O_4$-HBC-1000°C($N_2$) heated at 1000°C. Different HT-XRD peaks are also marked.**
(TIF)

**Figure S2 The variations in final or equilibrium pH of all the five adsorbents to remove As(V) (a) and As(III) (b) as a function of initial pH. (Experiment conditions: adsorbent dose = 0.02 g 100 $mL^{-1}$, temperature = 25±0.8°C, agitation speed = 150 rpm, initial concentration = 100 μg $L^{-1}$, contact time = 14 h).**
(TIF)

**Figure S3 (A and B) Pseudo-first-order (PFO) kinetics model for As(V) and As(III), (C and D) Pseudo-second-order (PSO) kinetics model of the adsorbent: a) $Fe_3O_4$-HBC uncalcined, b) 400 °C under air, c) 400 °C under nitrogen, d) 1000 °C under air, e) 1000 °C under nitrogen (Experiment conditions: initial concentraion = 100 μg $L^{-1}$, adsorbent dose = 0.02 g 100 $mL^{-1}$, pH 7, temperature = 25±0.8°C).**
(TIF)

**Table S1 Percentage (%) removal of As(V) and As(III) at different temperatures on calcined and uncalcined adsorbent composite. (Experimental conditions: adsorbent dose = 0.02 g 100 $mL^{-1}$, pH = 7.0, agitation speed = 150 rpm, initial concentration = 100 μg $L^{-1}$, contact time = 14 h).**
(DOCX)

## Acknowledgments

S.A. Baig acknowledges Chinese Scholarship Council (CSC) of the People's Republic of China for a PhD scholarship. Special thanks to Mr. and Mrs. Akash of Pharmaceutical Sciences College of Zhejiang University for editing this paper.

## Author Contributions

Conceived and designed the experiments: SAB TTS XHX. Performed the experiments: SAB TTS CS. Analyzed the data: SAB TTS XQX LST. Contributed reagents/materials/analysis tools: SAB TTS XQX CS. Wrote the paper: SAB XHX.

## References

1. Rehman K, Naranmandur H (2012) Arsenic metabolism and thioarsenicals. Metallomics 4: 881–892.
2. Mohan D, Pittman Jr CU (2007) Arsenic removal from water/wastewater using adsorbents-a critical review. J Hazard Mater 142: 1–53.
3. Gérente C, Andrès Y, McKay G, Le Cloirec P (2010) Removal of arsenic (V) onto chitosan: From sorption mechanism explanation to dynamic water treatment process. Chem Eng J 158: 593–598.
4. Katsoyiannis IA, Zouboulis AI (2002) Removal of arsenic from contaminated water sources by sorption onto iron-oxide-coated polymeric materials. Water Res 36: 5141–5155.
5. Baig SA, Sheng T, Hu Y, Lv X, Xu X (2013) Adsorptive removal of arsenic in saturated sand filter containing amended adsorbents. Eco Eng 60: 345–353.
6. Luo X, Wang C, Luo S, Dong R, Tu X, et al. (2012) Adsorption of As (III) and As(V) from water using magnetite $Fe_3O_4$-reduced graphite oxide-$MnO_2$ nanocomposites. Chem Eng J 187: 45–52.
7. Shan C, Tong M (2013) Efficient removal of trace arsenite through oxidation and adsorption by magnetic nanoparticles modified with Fe-Mn binary oxide. Water Res 47: 3411–3421.
8. Sheng T, Baig SA, Hu Y, Xue X, Xu X (2013) Development, characterization and evaluation of iron-coated honeycomb briquette cinders for the removal of As (V) from aqueous solutions. Arab J Chem 7: 27–36.
9. Wu K, Liu R, Li T, Liu H, Peng J, et al. (2013) Removal of arsenic (III) from aqueous solution using a low-cost by-product in Fe-removal plants-Fe-based backwashing sludge. Chem Eng J 226: 393–401.
10. Hering JG, Chen P-Y, Wilkie JA, Elimelech M, Liang S (1996) Arsenic removal by ferric chloride. J Amer Water Works Assoc 88: 155–167.
11. McNeill LS, Edwards M (1997) Predicting As removal during metal hydroxide precipitation. J Amer Water Works Assoc 89: 75–86.
12. Baig SA, Sheng T, Hu Y, Xu J, Xu X (2013) Arsenic removal from natural water using low cost granulated adsorbents: a review. CLEAN-Soil, Air, Water DOI: 10.1002/clen.201200466.
13. Seco-Reigosa N, Bermúdez-Couso A, Garrido-Rodríguez B, Arias-Estévez M, Fernández-Sanjurjo MJ, et al. (2013) As (V) retention on soils and forest by-products and other waste materials. Environ Sci Poll Res 1–10.
14. Gupta K, Bhattacharya S, Nandi D, Dhar A, Maity A, et al. (2012) Arsenic (III) sorption on nanostructured cerium incorporated manganese oxide (NCMO): A physical insight into the mechanistic pathway. J Coll Interf Sci 377: 269–276.
15. Badruzzaman M, Westerhoff P, Knappe DR (2004) Intraparticle diffusion and adsorption of arsenate onto granular ferric hydroxide (GFH). Water Res 38: 4002–4012.
16. Tian Y, Wu M, Lin X, Huang P, Huang Y (2011) Synthesis of magnetic wheat straw for arsenic adsorption. J Hazard Mater 193: 10–16.
17. Feng L, Cao M, Ma X, Zhu Y, Hu C (2012) Superparamagnetic high-surface-area $Fe_3O_4$ nanoparticles as adsorbents for arsenic removal. J Hazard Mater 217: 439–446.
18. Yue X, Li X-M, Wang D-B, Shen T-T, Liu X, et al. (2011) Simultaneous phosphate and $COD_{cr}$ removals for landfill leachate using modified honeycomb cinders as an adsorbent. J Hazard Mater 190: 553–558.
19. Johnson MC, Wang J, Li Z, Lew CM, Yan Y (2007) Effect of calcination and polycrystallinity on mechanical properties of nanoporous MFI zeolites. Mater Sci Eng A 456: 58–63.

20. Díaz-Parralejo A, Macías-García A, Ortiz AL, Cuerda-Correa EM (2010) Effect of calcination temperature on the textural properties of 3mol% yttria-stabilized zirconia powders. J Non-Crystall Solids 356: 175–178.
21. Mahmood T, Din S, Naeem A, Mustafa S, Waseem M, et al. (2012) Adsorption of arsenate from aqueous solution on binary mixed oxide of iron and silicon. Chem Eng J 192: 90–98.
22. Mücke A (2003) Fayalite, pyroxene, amphibole, annite and their decay products in mafic clots within Younger Granites of Nigeria: Petrography, mineral chemistry and genetic implications. J Afr Earth Sci 36: 55–71.
23. Sakthivel R, Jayasankar K, Das S, Das B, Mishra B (2011) Effect of planetary ball milling on phase transformation of a silica-rich iron ore. Powder Technol 208: 747–751.
24. Michel R, Ramzi Ammar M, Poirier J, Simon P (2012) Phase transformation characterization of olivine subjected to high temperature in air. Ceramics Internatl 39: 5287–5294.
25. Kurtoglu ME, Longenbach T, Reddington P, Gogotsi Y (2011) Effect of calcination temperature and environment on photocatalytic and mechanical properties of ultrathin sol-gel titanium dioxide films. J Amer Cer Soc 94: 1101–1108.
26. Shahar A, Young ED, Manning CE (2008) Equilibrium high-temperature Fe isotope fractionation between fayalite and magnetite: an experimental calibration. Earth Plan Sci Lett 268: 330–338.
27. Chandra V, Park J, Chun Y, Lee JW, Hwang I-C, et al. (2010) Water-dispersible magnetite-reduced graphene oxide composites for arsenic removal. ACS nano 4: 3979–3986.
28. Kołodyńska D, Wnętrzak R, Leahy J, Hayes M, Kwapiński W, et al. (2012) Kinetic and adsorptive characterization of biochar in metal ions removal. Chem Eng J 197: 295–305.
29. Ho Y-S (2004) Citation review of Lagergren kinetic rate equation on adsorption reactions. Scientometrics 59: 171–177.
30. Ho Y-S, McKay G (2000) The kinetics of sorption of divalent metal ions onto sphagnum moss peat. Water Res 34: 735–742.
31. Langmuir I (1918) The adsorption of gases on plane surfaces of glass, mica and platinum. J Amer Chem Soc 40: 1361–1403.
32. Ho Y, Huang C, Huang H (2002) Equilibrium sorption isotherm for metal ions on tree fern. Process Biochem 37: 1421–1430.
33. Chowdhury SR, Yanful EK (2010) Arsenic and chromium removal by mixed magnetite-maghemite nanoparticles and the effect of phosphate on removal. J Environ Manag 91: 2238–2247.
34. Zhang M, Gao B, Varnoosfaderon S, Hebard A, Yao Y, et al. (2012) Preparation and characterization of a novel magnetic biochar for arsenic removal. Bioresour Technol 130: 457–462.
35. Webi TW, Chakravort RK (1974) Pore and solid diffusion models for fixed-bed adsorbers. AIChE J 20: 228–238.
36. Zhang W, Singh P, Paling E, Delides S (2004) Arsenic removal from contaminated water by natural iron ores. Min Eng 17: 517–524.
37. Goldberg S (2002) Competitive adsorption of arsenate and arsenite on oxides and clay minerals. Soil Sc Soc Amer J 66: 413–421.
38. Weng C-H, Lin Y-T, Chang C-K, Liu N (2013) Decolourization of direct blue 15 by Fenton/ultrasonic process using a zero-valent iron aggregate catalyst. Ultras Sonochem 20: 970–977.
39. Meng X, Korfiatis GP, Bang S, Bang KW (2002) Combined effects of anions on arsenic removal by iron hydroxides. Toxicol Lett 133: 103–111.
40. Haarhoff J, Vessal A (2010) A falling-head procedure for the measurement of filter media sphericity. Water SA 36: 97–104.